

## Article

# Green Energy Harvesting and Management Systems in Intelligent Buildings for Cost-Effective Operation

Qingbin Dai <sup>1</sup>, Jingui Qian <sup>2</sup> , Shun Li <sup>2,\*</sup> and Li Tao <sup>3,\*</sup><sup>1</sup> VANYANG CONSTRUCTION GROUP Co., Ltd., Wenzhou 325006, China<sup>2</sup> School of Instrument Science and Opto-Electronics Engineering, Hefei University of Technology, Hefei 230009, China<sup>3</sup> School of Civil Engineering and Architecture, Wenzhou Polytechnic, Wenzhou 325035, China

\* Correspondence: 2021170061@mail.hfut.edu.cn (S.L.); 2001040019@wzpt.edu.cn (L.T.)

**Abstract:** Nowadays, the rise of Internet of Things (IoT) devices is driving technological upgrades and transformations in the construction industry, the integration of IoT devices in buildings is crucial for both the buildings themselves and the intelligent cities. However, large-scale IoT devices increase energy consumption and bring higher operating costs to buildings. Therefore, harvesting the ambient cost-effective and clean energy sources is essential for the future development of intelligent buildings. In this work, we investigate the feasibility of integrating a typical triboelectric droplet energy harvester (DEH) into buildings. We demonstrate the energy harvesting capabilities of DEH on different sloped roof surfaces and complex curved building surfaces by simulating rainy weather with various rainfall intensities. The results indicate energy harvesting efficiency increases with larger tilt angles, which guides future smart architectural designs. This work is significant for the future integration of diversified, all-weather green energy collection and management systems, including raindrop energy, wind power generation, and solar energy, which will contribute to energy conservation and cost control in the next generation of smart buildings.

**Keywords:** intelligent building; green energy harvesting; cost-effective; raindrops; triboelectrification



**Citation:** Dai, Q.; Qian, J.; Li, S.; Tao, L. Green Energy Harvesting and Management Systems in Intelligent Buildings for Cost-Effective Operation. *Buildings* **2024**, *14*, 769. <https://doi.org/10.3390/buildings14030769>

Academic Editors: Hazim B. Awbi, Eusébio Z.E. Conceição and Antonio Caggiano

Received: 22 December 2023

Revised: 29 January 2024

Accepted: 10 March 2024

Published: 12 March 2024



**Copyright:** © 2024 by the authors. Licensee MDPI, Basel, Switzerland. This article is an open access article distributed under the terms and conditions of the Creative Commons Attribution (CC BY) license (<https://creativecommons.org/licenses/by/4.0/>).

## 1. Introduction

The integration of Internet of Things (IoT) technology in the construction sector has become an inevitable trend, enabling the creation of intelligent buildings with perceptual and executive capabilities [1–3], which serve as essential components in the establishment of smart cities [4–6]. For instance, building developers leverage IoT sensors and actuators to construct intelligent buildings that enhance user convenience [7,8] and ensure maximum customer satisfaction and cost optimization while continuously striving to provide superior services to their clientele [9–11]. Meanwhile, the introduction of the IoT is crucial for enhancing operational efficiency [12,13]. IoT is assisting building companies in streamlining their processes to minimize waste and save costs [14]. Specifically, by utilizing IoT sensors, construction firms can optimize equipment performance, enabling the identification of equipment health status and taking preventive measures to avoid expensive equipment replacements and extended project delays [15–17].

However, the construction of large-scale sensor networks in smart buildings, along with the processing of related data and the potential need for cloud computing technologies, requires additional energy support. This, in turn, adds complexity to the entire building system, resulting in a significant increase in operational costs [18,19]. Therefore, it is imperative to investigate advanced techniques for efficient green energy harvesting and management in smart buildings, which should be seamlessly integrated into existing energy systems, working collectively towards the energy-saving and environmentally conscious objectives of smart buildings, thereby mitigating operational expenses [20]. To diminish dependence on conventional energy sources, it becomes essential to explore economically

viable and environmentally friendly energy alternatives in the surrounding environment, such as wind, solar, and raindrop energy; all are abundant energy sources [21]. The harvesting and utilization of multiple micro-energy sources offer advantages over relying solely on a single energy type; this not only enhances the energy harvesting efficiency of the environment but also enables smart buildings to collect energy under different weather conditions [22]. For example, solar energy collection achieves maximum benefits in sunny weather with ample sunlight, while wind and raindrop energy collection can be optimized even in harsher weather conditions. For example, research by Wang's group [23] combined triboelectric nanogenerators (TENGs) and photovoltaics (PVs) to enhance energy harvesting on rainy and sunny days, and Mehrjerdi's [24] research proposed a nearly zero-power-consumption solution for buildings, harvesting water, wind, and solar energy to adapt to various weather conditions and minimize environmental impact, thus ensuring sustainable energy without hindering urban development and thereby promoting energy efficiency and cost-effectiveness [25,26]. As shown in Figure 1, the envisioned green building integrates a wind power generator, solar panels, and raindrop energy collector; the collected energy can be stored in an energy management and storage module, and a portion of the harvested micro-energy from the environment can be allocated to the IoT sensors and actuators within the building to enhance the user experience. Outfitting every city building with micro-energy collectors can provide power for smart buildings and contribute to said city's grid, supporting public infrastructure like traffic lights. This promotes energy efficiency and enhances the overall smart development of cities.

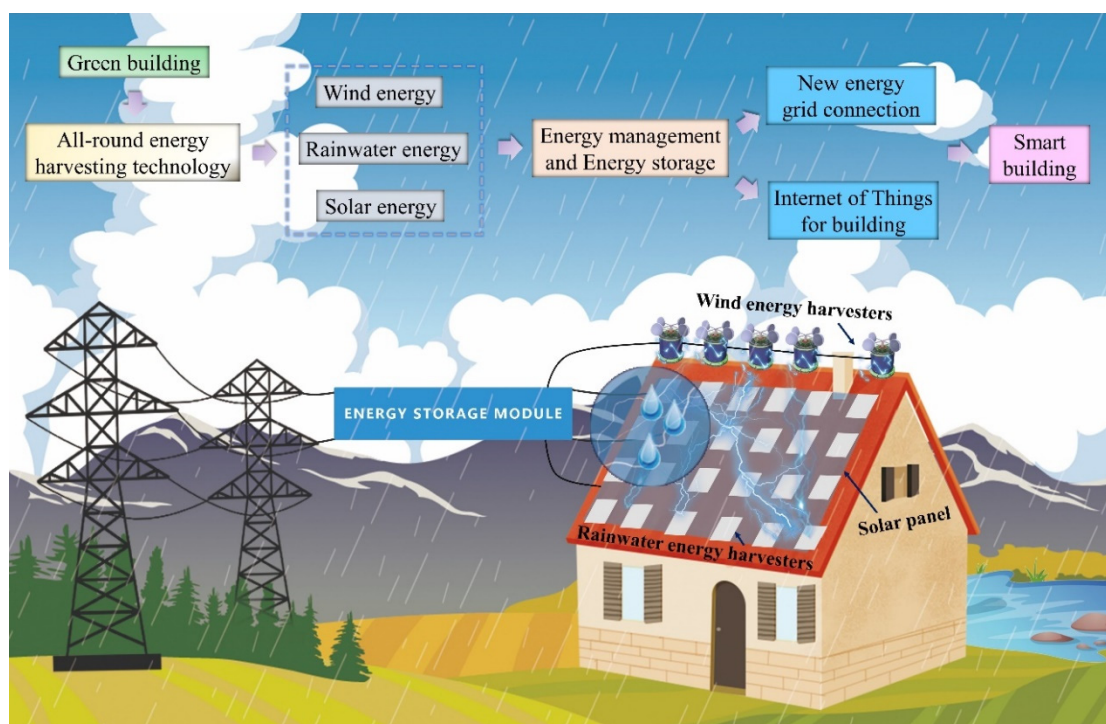


**Figure 1.** Illustration of green energy harvesting and management systems in intelligent buildings.

Indeed, while wind power generation and solar energy collection in buildings have been extensively studied and practically applied, the integration of raindrop energy collection in smart buildings still lacks sufficient research and faces several challenges [27–30]. These challenges include selecting the energy conversion method, designing and optimizing the energy collectors, and determining how the collectors and the building can collaborate to maximize energy conversion efficiency [31]. Therefore, researching the integration and utilization of raindrop energy in buildings can make a significant contribution to the development of green buildings. Currently, typical methods for raindrop energy collection primarily include piezoelectric droplet energy harvesters and micro-scale water

turbines; piezoelectric raindrop energy harvesting, though currently less efficient, is suitable for low-power devices. PVDF stands out as a superior material due to its lead-free nature, cost-effectiveness, and lightweight properties. Ideal raindrop harvesters should be resistant to sunlight, waterproof, wind-resistant, and highly sensitive to raindrops [32,33]. Micro-turbines, despite their complexity and higher costs, offer a relatively high return on investment as energy-saving rainwater collectors [34]. In recent years, a class of energy harvesters based on the liquid–solid surface contact electrification, called triboelectric nanogenerators (TENGs), have been introduced [28,29,35,36]. TENGs are based on the principles of triboelectricity and electrostatic induction, effectively converting the mechanical energy from falling droplets into electrical energy, which is considered a promising technology for harvesting mechanical energy from raindrops [29,37]. However, current research on TENGs' collection of mechanical energy from droplets focuses on optimizing the TENG structure and studying the fluid dynamics of droplets on TENGs, as well as the establishment of related electrophysical models. When TENGs are to be integrated into green buildings as part of an IoT sensor network, their output amplitude is influenced by external factors and its carrier, including the shape and material properties of the building surface, as well as the velocity and shape of the raindrops [38]. Therefore, it is crucial to consider the organic integration between the TENG and the building. Consequently, studying the performance of TENGs on the rooftops of buildings holds significant importance in reducing the operational costs of green buildings, effectively addressing key challenges in integrating green concepts into traditional buildings such as cost concerns, increased energy consumption, and a lack of attention and data [39]. This study showcases the economic value of green buildings with nanogenerators, offering innovative solutions [40], thus effectively providing new solutions for the construction of green buildings. Additionally, this provides crucial data on nanogenerator performance across different building surfaces and rainfall levels, addressing the scarcity of practical datasets for green buildings' development.

Therefore, in this study, we investigated the power generation effectiveness of a typical single-electrode structured TENG droplet-based electrostatic harvester (DEH) on various types of buildings' rooftop surfaces. This research provides a solid foundation for the future integration of TENG in practical buildings. The experiments demonstrated that for standard pentroof surfaces, the output amplitude and raindrop energy collection capacity of DEH increase significantly as the roof inclination angle becomes steeper, but when considering real rooftop configurations, a balance should be struck between the energy collection capacity of DEH and the optimization of the roof's architectural design. Furthermore, to explore the adaptability of DEH, its output performance on various unconventional roof surfaces was also investigated. The experiments revealed that due to the flexibility of DEH, it can still function well and collect energy when configured on curved surfaces of different architectural shapes. Among the selected unconventional roof surface, DEH performed best on the surface of a dome building, guiding the future deployment of DEH on natural architectural rooftops. Finally, to visually demonstrate the energy collection capability of DEH, the output of the DEH array was rectified and directly connected to commercial capacitors. The output of DEH allowed the commercial capacitors to reach a significant steady-state voltage within a limited period, and the energy collection capacity of DEH on various surfaces could be directly observed from the charging curves. This series of characterizations provides practical data references for future builders who intend to integrate DEH into building surfaces, which can effectively support the development of green buildings.

## 2. Materials and Methods

### 2.1. Fabrication of the DEH

As shown in Figure 2a, the DEH is typically present in an array form when installed on the surface of the roof. The DEH unit consists of three main components: polytetrafluoroethylene film (e.g., PTFE, the friction layer), a Cu layer (playing two roles as the conductive electrode and electrification layer), and the wires (in direct contact with the Cu

electrode and external circuit). As illustrated in Figure 2b, the working mode of DEH is single-electrode mode, which has a lower configuration cost and fewer types and quantities of raw materials compared with several other modes (e.g., two-electrode mode, translational sliding mode, and rolling friction mode). Firstly, (a) the double-sided tape is fixed on the surface of the top plate model, (b) the exposed part of the stripped wire is attached to the center of the double-sided tape, and (c) the non-stick side of the copper foil is directly attached above the double-sided tape, thus forming a double-sided tape–wire–copper foil sandwich structure. Next, (d) a PTFE film slightly larger than the size of the copper foil is then attached to the copper foil (e.g., the adhesive surface ensures the full contact). Multiple DEH units are replicated, and these units are combined to form an array, maximizing the energy conversion efficiency of DEH as the output of DEH depends on the output amplitude of an individual device, which allows the array mode to achieve a significantly greater number of pulse peaks compared to a large-area DEH with the same footprint; thus, the energy harvesting capability and efficiency of DEH is significantly enhanced. Furthermore, the arrangement of DEH should be chosen to implement a densely tiled array structure in terms of geometry, which maximizes the utilization of the limited building surface area. The dimensions of the Cu electrode are 2 cm in length and 1.5 cm in width, while the dimensions of PTFE are 3.5 cm in length and 2 cm in width. When configuring the DEH on an actual roof, its dimensions should be determined by considering both the dimensions of the droplets and the actual size of the roof [41]. Generally, the dimensions of the DEH should be slightly larger than the area when the droplets are fully spread out. The optical image of the fabricated DEH installed on the roof was captured in Figure 2c.

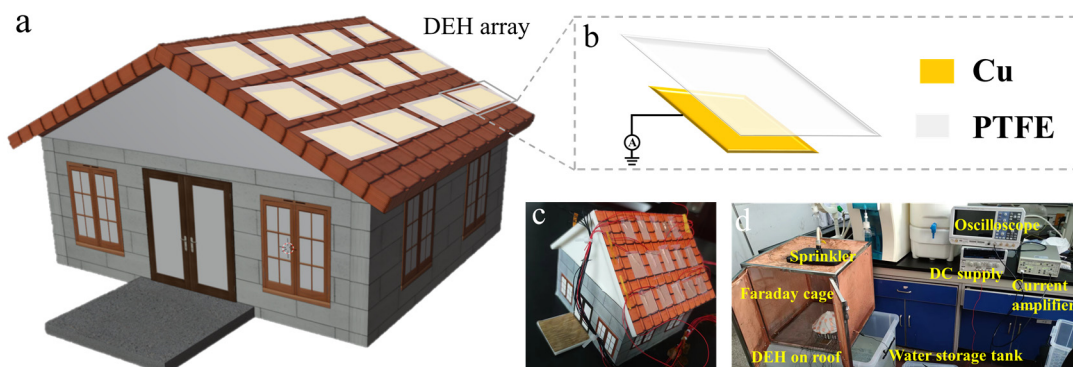


**Figure 2.** (a,b) 3D structural diagram of DEH and schematic of roof installation. (c) Physical diagram of DEH installed on the roof. (d) Photograph of electrical testing apparatus.

## 2.2. Experimental Setup

The experimental system was constructed to accurately measure the output of DEH, as illustrated in Figure 2d. Various housing models integrated with DEH were positioned inside a Faraday cage. A sprinkler located above the Faraday cage, with an inclined length of 13 inches, supplied droplets. The DEH surface of the model was reached as droplets permeated through micro-holes on the top of the Faraday cage. The sprinkler was connected to the laboratory's tap water source. The Faraday cage was placed on top of a reservoir to collect the droplets falling from the model. It was grounded by connecting it to the ground of a DC power supply, effectively reducing power frequency interference from the surrounding space. The output voltage of the DEH units was measured using a probe from an oscilloscope (RTB2004, Rohde & Schwarz, Munich, Germany), with one end of the probe suspended and directly connected to the ground of the oscilloscope. The output current, on the other hand, was first amplified by a current amplifier (SR570, Stanford Research Systems, Sunnyvale, CA, USA) and then measured by converting the voltage readings from the oscilloscope. It should be noted that the Faraday cage reduces interference from power frequency through its conductive shell, reflecting and absorbing electromagnetic waves. Grounding is crucial, providing a path for excess charges to dissipate into the

ground, thereby preventing internal charge buildup. This grounding eliminates power frequency interference, ensuring reliable and accurate experimental measurements within the shielded environment [42].

### 3. Results and Discussion

#### 3.1. Working Mechanism of DEH

As plotted in Figure 3a, the working mechanism of DEH is based on the principles of triboelectric charging and electrostatic induction that occur between the liquid droplets and the thin film. In the initial stage, continuous friction between the liquid droplets and PTFE (polytetrafluoroethylene) results in the pre-charging of PTFE with positive charges and induces an equal amount of positive charges on the Cu electrode surface. In the second stage, when the liquid droplets come into contact with the PTFE, due to the high electronegativity of PTFE, they gain electrons while the droplets lose electrons. This causes electrons to flow from the ground to the Cu electrode until an equilibrium is reached in the electric field among the three components (e.g., red arrows). At this point, the electron flow ceases. In the third stage, as the liquid droplets continue to slide on the PTFE film, no electron exchange occurs, and therefore, there is no electron flow through the electrostatic voltmeter. During this process, the voltmeter does not show any reading. In the fourth stage, once the droplets separate from the friction layer, electrons flow from the Cu electrode to the ground (e.g., red arrows), resulting in an opposite current compared to the second stage. This entire process harnesses the mechanical kinetic energy of the liquid droplets. With a continuous supply of droplets, the DEH achieves periodic and sustained output [43].

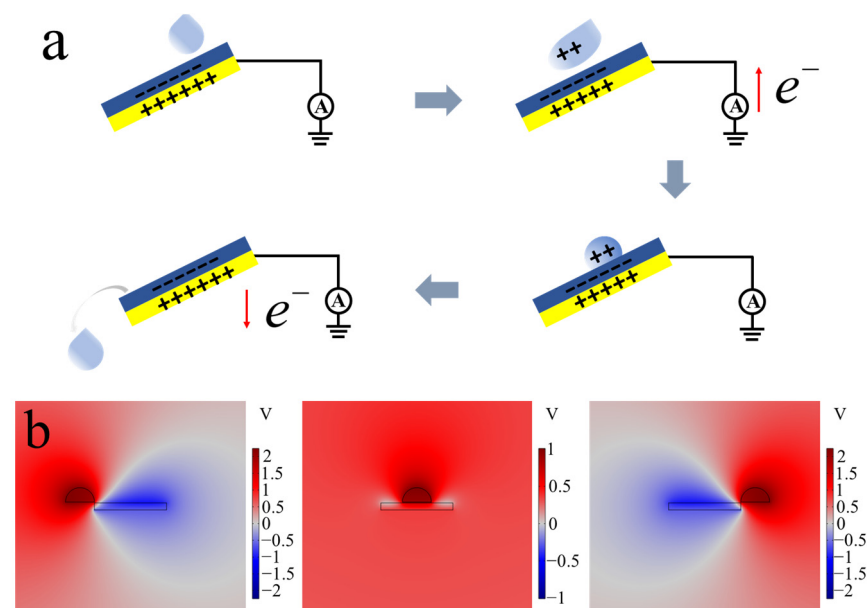


**Figure 3.** (a) Schematic illustrations of the working principle of the DEH based on single electrode mode with four processes. (b) Numerical simulation of electric field intensity with three different moments.

As simulated in Figure 3b, moreover, the electric field distribution of DEH in the initial, intermediate, and final states has been analyzed using the finite element simulation software COMSOL 6.0. The surfaces of the droplets and PTFE are endowed with surface charge densities consistent with reality and the simulation results indicate that PTFE exhibits strong electronegativity, while there is a significant amount of positive charge on the surface of the droplets. As the droplets slide on the PTFE surface, the overall electric potential continuously changes, leading to the flow of electrons between the Cu electrode and the ground [44].

### 3.2. Electrical Output Performance of the DEH in Different Conditions

The primary objective of this study is to explore the feasibility of integrating DEH with architectures. Therefore, we first examined the potential application of the DEH on commonly encountered standard pentroof building surfaces in real-life scenarios. As shown in Figure 4a, we utilized 3D printing technology to create models of standard pentroof buildings with incline angles of  $100^\circ$ ,  $120^\circ$ ,  $150^\circ$ , and  $180^\circ$ . Subsequently, DEH was installed on the rooftops. The voltage and current generated by the DEH at different roof angles are depicted in Figure 4b,c. The maximum voltage ( $V_{pp}$ ) and current values were observed at an incline angle of  $100^\circ$ , reaching 47.49 V and 6.856  $\mu\text{A}$ , respectively. Both voltage and current decreased as the incline angle increased. This can be attributed to the fact that at smaller angles, the contact between the droplets and PTFE is more substantial, leading to more efficient electron exchange and charge transfer. Consequently, the voltage and current values significantly increased. The minimum voltage and current values were observed at an incline angle of  $180^\circ$ , measuring 4.986 V and 0.335  $\mu\text{A}$ , respectively. At  $180^\circ$ , there is only a collision between the droplets and PTFE without sliding, resulting in very limited output amplitude. This indicates that when configuring DEH on the roof surface, a relatively small roof incline angle should be chosen to maximize the energy conversion efficiency of DEH. However, it is also essential to consider practical architectural design aspects; a comprehensive evaluation, taking various factors into account, is necessary.

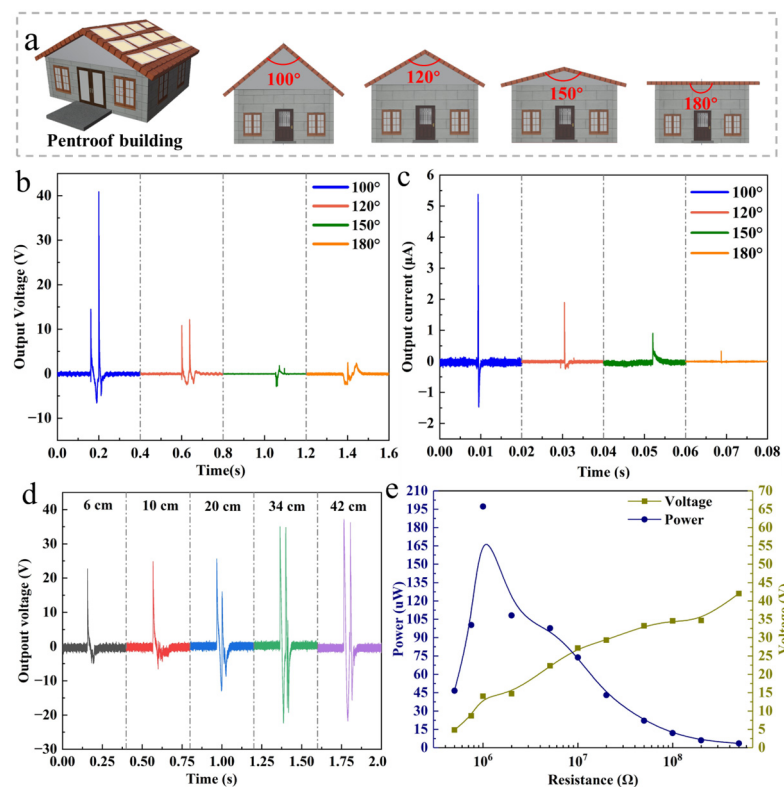


**Figure 4.** (a) Schematic diagram of differently angled standard pentroof buildings roof designs and DEH installations. (b,c) Output voltage and current curves of DEH. (d) Output voltage of DEH at different rainfall heights. (e) Impedance matching of DEH.

In addition to the inclination angle of the building, the height of the liquid droplet impact is another important parameter that affects the output of the DEH. The height of the droplet impact directly influences the frictional velocity between the droplet and the PTFE surface, thereby affecting the output amplitude of the DEH. Therefore, in the aforementioned study, the roof with the optimal inclination angle of  $100^\circ$  was chosen for conducting experiments at various droplet impact heights. The results shown in Figure 4d indicate that the output voltage ( $V_{pp}$ ) of the DEH increases with increasing droplet impact

height, ranging from 27.74 V at a height of 6 cm to 58.99 V at a height of 42 cm. This suggests that the frictional velocity between the droplet and the PTFE film significantly influences the output amplitude of the DEH, and a higher velocity results in a larger output amplitude of the DEH. This can be attributed to the fact that when the droplet impacts the surface at a higher velocity, the droplet spreads more fully on the PTFE surface, leading to an enhanced electron transfer and exchange rate, thereby increasing the output amplitude of the DEH. In essence, the effect of droplets on the DEH output predominantly relies on the kinetic energy of the droplets. The fundamental nature of the friction-induced electrification process is the conversion of the mechanical energy of the droplets into kinetic energy. The greater the mechanical energy of the droplets, the higher the output of the DEH [41].

The load characteristics of the DEH, as an energy harvester, need to be given special attention. Therefore, the DEH's electrode is connected to a resistor, with the other end of the resistor grounded. The probe of the oscilloscope is connected to the segment between the resistor and the DEH for measurement. The resistance value of the external resistor ranges from 500 k $\Omega$  to 500 M $\Omega$ . The results obtained, as shown in Figure 4e, indicate that the output voltage of the DEH increases with an increase in the external resistor. The output power reaches its peak when the external resistor has a resistance value of 1 M $\Omega$ , measuring 197  $\mu$ W, which suggests that the internal resistance of the DEH is 1 M $\Omega$ . The DEH can be considered an equivalent of a power source with internal resistance. According to Ohm's law in a closed circuit, when the load resistance of DEH is increased, the voltage drop across the resistance is also increased. However, the output power of DEH, which is the power across the load resistance, can only reach its maximum when it is equal to the internal resistance of DEH. Our experimental results demonstrate that the internal resistance of DEH is 1 M $\Omega$ . This implies that if the maximum output power of DEH is desired, a load resistance that matches the internal resistance needs to be selected. Similarly, if the aim is to maximize the output voltage of DEH, a higher load resistance can be chosen. The significance of conducting impedance matching experiments is to gain a better understanding of the output performance of DEH and to maximize its energy harvesting capabilities. By choosing the appropriate load resistance, the energy harvesting capacity of DEH can be efficiently utilized. The importance of impedance matching experiments allows for a better understanding of the output performance of DEH and the maximization of its energy harvesting capabilities. The selection of an appropriate load resistance enables the efficient utilization of the DEH's energy collection capacity. It demonstrates that the DEH, as an ambient micro-energy harvester, can effectively convert the mechanical energy from droplet impact into electrical energy and collect it, and the collected energy can be used to power Internet of Things (IoT) devices in buildings, thereby reducing the reliance on external energy sources. This has the potential to make significant contributions to the greening and decarbonization of smart cities.

### 3.3. DEH Energy Harvesting Ability on a Complex Roof

In the real world, roofs come in various shapes, which are products of human architectural design. Exploring the application of DEH on multiple roof types holds practical importance. Therefore, several unconventional roof shapes, namely classical buildings, dome buildings, and tower buildings (Figure 5a–c), were fabricated using 3D printing technology. Subsequently, DEHs were installed on the surfaces of these unconventional roof surfaces, and the output voltage and current on each surface were measured (Figure 5d,e). Among the unconventional roof surfaces, the classical building roof exhibited the smallest output voltage amplitude (19.57 V) and corresponding current (2.83  $\mu$ A). Conversely, the DEH on the dome buildings' curved surface of the architectural roof showed the highest output voltage (56.35 V) and current (10.37  $\mu$ A). This indicates that the uneven characteristics of the classical buildings' tower buildings surface adversely affect the DEH's power generation performance. Notably, the tower building roof also demonstrated favorable performance, with an output voltage of 48.63 V and a current of 7.07  $\mu$ A. These findings

highlight the DEH's flexibility to adapt to various complex roof surfaces, showcasing its robustness.

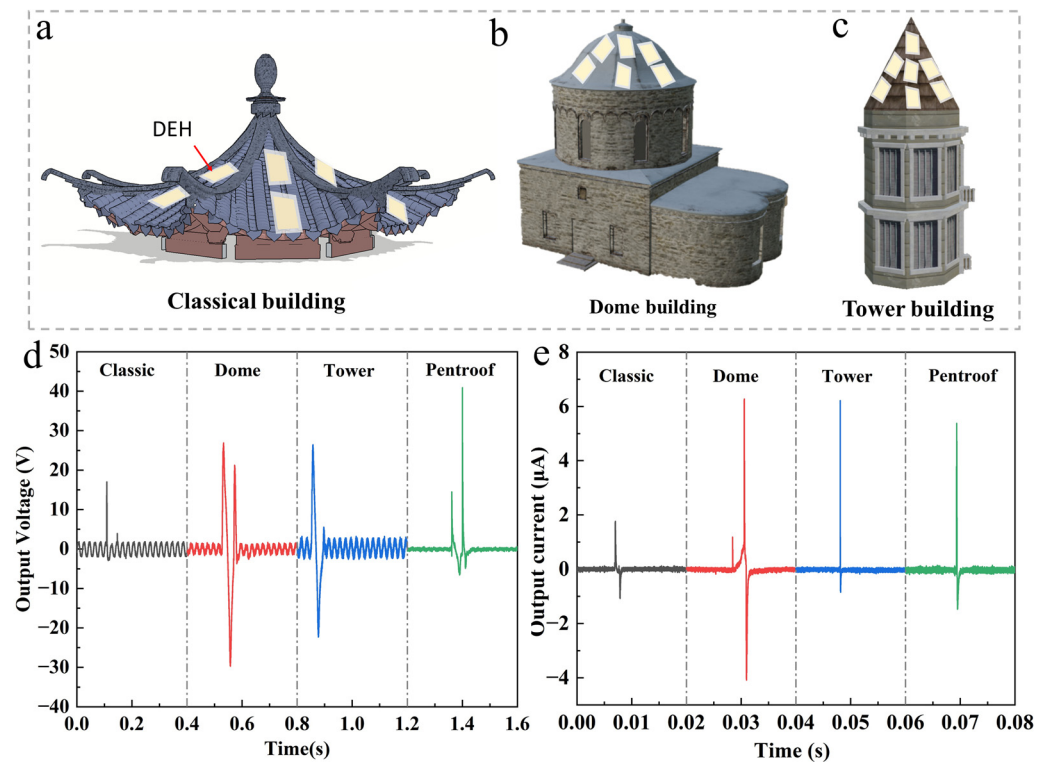


**Figure 5.** (a–c) Schematic diagram of different roof shapes design and DEH installation. (d,e) Output voltage and current curves of DEH installed on different roof shapes.

### 3.4. Energy Harvesting Quantification

The above experimental results show the output characteristics of surfaces on different types of roofs, providing valuable guidance for the configuration of the DEH. Meanwhile, quantifying the collected power is essential for DEH as an environmental micro-energy harvesting form. Therefore, based on the aforementioned experimental outcomes, the output power of inclined roofs and irregularly shaped roofs at different angles was computed using Equation (1):

$$w = \frac{V_{pp}I}{2} \quad (1)$$

where  $V_{pp}$  is the difference between the positive and negative peak values of the DEH output voltage, and  $I$  is the short-circuit output current of the DEH. Dividing by two then balances the significant difference in positive and negative peak values on certain building surfaces, ensuring that both positive and negative output data of the DEH are effectively accounted for. Obtained results are shown in Figure 6a,b. When DEHs were configured on inclined roofs at angles of  $100^\circ$ ,  $120^\circ$ ,  $150^\circ$ , and  $180^\circ$ , the instantaneous peak output power per single droplet was recorded as  $81.6 \mu\text{W}$ ,  $7.234 \mu\text{W}$ ,  $1.08 \mu\text{W}$ , and  $0.42 \mu\text{W}$ , respectively. However, when configured on surfaces of classical buildings, dome buildings, and tower buildings (with various irregular shapes), the instantaneous output power was recorded as  $12.14 \mu\text{W}$ ,  $146.6 \mu\text{W}$ , and  $86.3 \mu\text{W}$ . Thus, the experimental findings of this study demonstrate that the instantaneous output power density of a single DEH can optimally reach  $0.21 \text{ W/m}^2$ , which is derived by dividing the output power obtained from the dome roof surface by the area of a single DEH unit. This calculation assumes a tightly packed arrangement of DEH units on the roof surface, without any mutual interference in output. Under this configuration, the energy harvesting power per square meter of the roof surface can reach  $0.21 \text{ W}$ . Nevertheless, it is worth noting that this value represents the utmost output power achieved in our experiments. In future practical configurations,

the output power could potentially surpass this level. To further investigate the energy harvesting capabilities of the DEH and its practical raindrop energy collection potential, we increased the water flow rate to simulate natural rainfall conditions. All DEH units installed on standard pentroof buildings roofs were interconnected via a rectifier bridge and connected to a commercial capacitor of  $4.7 \mu\text{F}$ . The obtained results, as shown in Figure 6c, revealed that at water flow rates of  $9 \text{ mL/s}$ ,  $45 \text{ mL/s}$ , and  $64 \text{ mL/s}$ , the steady-state voltage across the commercial capacitor within  $150 \text{ s}$  reached  $1 \text{ V}$ ,  $0.4 \text{ V}$ , and  $0.2 \text{ V}$ , respectively. This suggests that higher rainfall intensity leads to a less effective charging process due to the alignment of water droplets, which adversely affects the triboelectric charging process. For all roof shapes (Figure 6d), under a rainfall rate of  $45 \text{ mL/s}$ , the steady-state voltages achievable within  $150 \text{ s}$  for classical buildings, standard pentroof buildings, dome buildings, and tower buildings were measured at  $0.14 \text{ V}$ ,  $0.4 \text{ V}$ ,  $0.76 \text{ V}$ , and  $1.06 \text{ V}$ , respectively. These findings collectively indicate that the DEH exhibits a promising ability to harness raindrop energy effectively in environmental conditions. Thus, energy harvesting quantification establishes a practical foundation for the development of DEH integration in green building applications and provides a clear dataset supporting the integration of a DEH on the building surface.

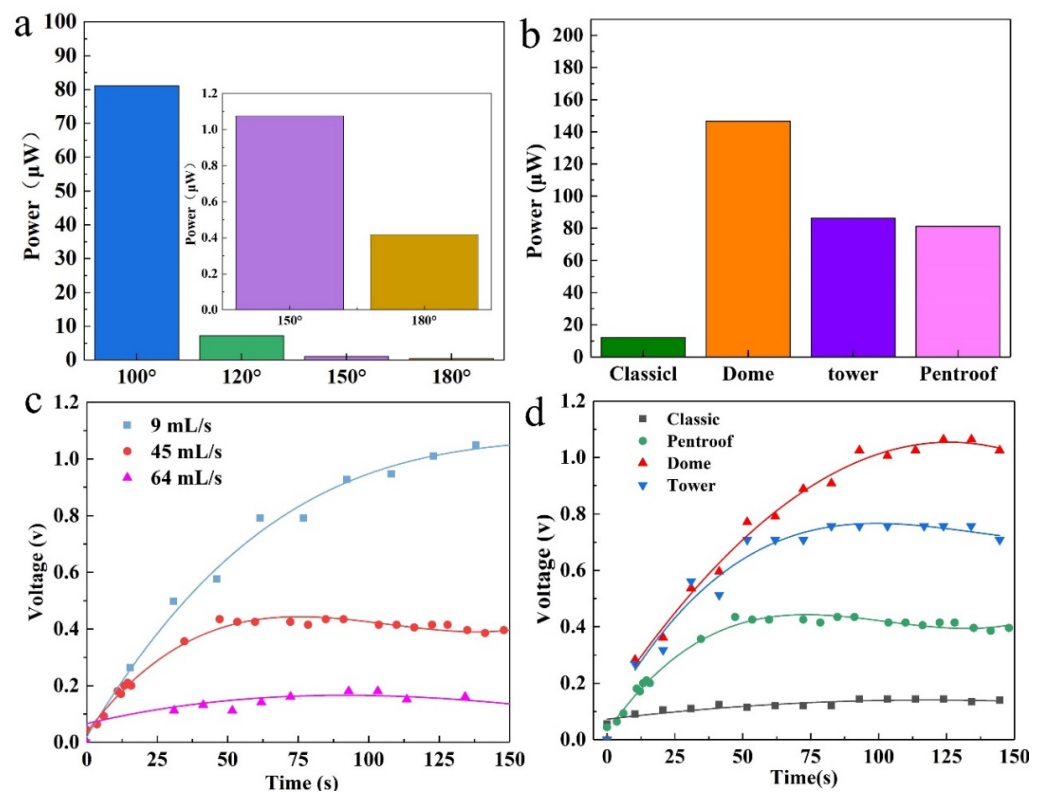


**Figure 6.** (a,b) Output power of DEH installed on the pentroof with different angles and different shapes of roofs (rainfall rate:  $45 \text{ mL/s}$ ). (c) Charging voltage curve of DEH with different rainfall rates (pentroof building roof) for a capacitor of  $4.7 \mu\text{F}$ . (d) Charging voltage curve of DEH on different roof shapes (same rainfall rate) for a capacitor of  $4.7 \mu\text{F}$ .

#### 4. Discussion

In this study, a water droplet energy harvester (DEH) based on the TENG was deployed on urban building rooftops to explore its energy harvesting capabilities across different roof types. We describe herein the design and experimental simulation of the DEH, including the energy harvesting principles of the DEH and its performance on pentroof surfaces at different angles as well as various irregular roof surfaces. The energy harvesting performance of DEH with different rainfall levels is also characterized. The findings provide valuable insights for the future development of smart and energy-efficient

urban buildings. Additionally, it offers potential solutions for addressing energy consumption in future constructions. This provides architects and builders with a reliable guide for integrating distributed energy harvesting into next-generation roofs, fostering eco-friendly energy solutions for sustainable construction and development.

As a pioneer, Wang's [42] research elucidated the electron exchange and power generation principles between droplets and polymer films as well as the electrical sequences in solid polymer films. The progress made by previous significant studies in the area of DEHs is summarized in Table 1.

**Table 1.** Previous significant studies on DEH.

Type of DEH	Contribution	Year	Ref.
TENG with a top electrode	The practical value of TENG in the construction of smart buildings was demonstrated.	2021	[45]
Single-electrode mode TENG	The feasibility of TENG on a single roof surface was demonstrated.	2022	[46]
TENG with a top electrode	TENG was demonstrated to organically integrate with existing energy harvesters.	2022	[47]
Integrated TENG with multiple top electrodes	Demonstrated that TENG with complex structures can be integrated on rooftops for energy harvesting.	2023	[48]
This work	The potential and performance of various rooftop integrations were demonstrated by employing the simplest TENG structure.	2024	-

Various optimization strategies are being sought out to enhance the DEHs' output performance and environmental stability if needed. For instance, thinner PTFE films and higher-purity Cu foils can be utilized to increase the magnitude of output, since the higher purity of Cu foil facilitates smoother electron flow between the Cu foil and the ground, effectively reducing unnecessary energy loss. Alternatively, developing new device structures capable of maintaining higher magnitudes of output without accumulating sufficient surface charges can improve the device's output stability [49]. Furthermore, developing corresponding means to enhance the waterproofing of DEH can bolster its environmental stability and durability, which significantly influences the lifespan and energy harvesting efficiency of DEH as a micro-energy harvester. Since the surface of DEH units needs to come into direct contact with droplets, it is advisable to consider incorporating sealable materials between the gaps of the DEH units to prevent water from penetrating the interior. This can effectively enhance the environmental stability of DEH. Simultaneously, introducing a self-cleaning coating on the surface of DEH can further improve its waterproofing and environmental stability without affecting its output.

Moreover, the concept of a smart, energy-efficient city encompasses multiple elements requiring significant efforts for refinement. For example, artificial intelligence algorithms can be integrated, allowing DEH not only to collect energy but also to analyze raindrop output signals to monitor compound concentrations within raindrops and subsequently assess environmental pollutant levels. If employing AI algorithms for environmental monitoring, a more efficient and precise method of acquiring genuine environmental parameters is essential. These acquired data should be designated "tags". Concurrently, DEH data, encompassing waveform and peak values of pulse signals, need to be recorded. This dataset, corresponding to the designated "tags", constitutes the dataset for monitoring environmental parameters utilizing DEH [50]. Subsequently, AI algorithms undergo training using this dataset to enhance recognition accuracy. Upon the completion of initial preparations, employing DEH for authentic parameter measurements involves inputting DEH outputs into the AI algorithm for identification. Subsequently, the algorithm can generate pertinent environmental data based on its acquired knowledge [51]. By uploading these data to the

cloud, potential sources of pollution within the city can be identified, and trends in air quality can be predicted; this allows for targeted management of pollution sources, thereby safeguarding human health. It can effectively preserve ecological balance and the health of ecosystems. Reliable air quality forecasts are instrumental in formulating more scientifically informed urban planning and traffic management strategies, consequently reducing air pollution. Simultaneously, they provide ample warnings to the public, enabling people to take necessary preventive measures [52]. These outcomes can offer decision making support to urban managers, aiding in the implementation of intelligent and effective environmental protection and governance strategies. Such intelligent management practices can enhance the city's operational sustainability and provide residents with a more comfortable and healthier living environment, because implementing intelligent management strategies not only benefits the improvement of air quality and enhances energy efficiency but also promotes urban greening and the rational planning of public spaces, thus providing more areas for city residents. Additionally, efficient utilization of urban energy can be further achieved through an intelligent energy management system. Additionally, collected energy can be supplied to power smart transportation systems. In summary, as a component of a smart city, DEHs can provide a micro-energy supply, contributing to the city's intelligence, sustainable development, and energy efficiency.

At the same time, DEHs also have some limitations. In practical applications, DEHs face challenges related to durability, energy storage, and the impact of low-cost raw materials on performance. Prolonged exposure to rain weakens energy harvesting. Developing superior materials and cost-effective structures is crucial. Addressing energy storage challenges with cost-effective solutions is vital for integrating DEH in green urban environments.

## 5. Conclusions

In summary, a raindrop energy harvester based on the triboelectric effect is proposed for constructing smart green buildings. The performance of the DEH on standard pentroof buildings at various inclinations is investigated, along with droplet outputs at different heights. Results from the impedance matching analysis of the DEH indicate that with an external resistance of  $1\text{ M}\Omega$ , the maximum instantaneous output power of DEH reaches  $197\ \mu\text{W}$ . Subsequently, the energy harvesting capability of DEHs on various irregular and curved surfaces is validated. Among the selected irregular architectural shapes, the dome-shaped building roof demonstrates optimal performance, while other irregular surfaces also exhibit favorable output characteristics. This demonstrates DEHs' flexible nature which allows them to function effectively on diverse complex roof surfaces. To concretely demonstrate the potential practical application of DEHs, the harvested energy is used to charge a commercial capacitor. Experimental results confirm that DEHs collect substantial mechanical energy from raindrops within a few minutes. In summary, this work optimizes droplet energy harvesting on rooftops, highlighting its superior performance on standard pentroof surfaces with steeper inclinations. DEHs also prove effective on irregular roof surfaces, but may face limitations during heavy rainfall. Valuable insights are provided for architects and builders looking to integrate DEHs into next-generation roofs, promoting seamless integration with eco-friendly micro-energy harvesters and contributing to the sustainable development of the construction industry. Moreover, DEHs' significant energy harvesting capability holds promise for substantial contributions in shaping future smart cities.

**Author Contributions:** Conceptualization, Q.D. and L.T.; Investigation, Q.D., J.Q. and S.L.; Methodology, L.T. and S.L.; Formal analysis, J.Q.; Supervision, J.Q.; Writing—original draft, Q.D. and S.L.; Writing—review and editing, L.T. and J.Q. All authors have read and agreed to the published version of the manuscript.

**Funding:** This research was supported by the Major Teaching Reform Project of Wenzhou Polytechnic (No. WZYBKZD202202) and the Curriculum Ideological and Political Teaching Research Project of the Zhejiang Provincial Department of Education (Zhe Jiao Han [2022] 51) (Project No. 361).

**Data Availability Statement:** The original contributions presented in the study are included in the article, further inquiries can be directed to the corresponding authors.

**Conflicts of Interest:** Author Qingbin Dai was employed by the company VANYANG CONSTRUCTION GROUP Co., Ltd. The remaining authors declare that the research was conducted in the absence of any commercial or financial relationships that could be construed as a potential conflict of interest.

## References

1. Santoro, G.; Vrontis, D.; Thrassou, A.; Dezi, L. The Internet of Things: Building a knowledge management system for open innovation and knowledge management capacity. *Technol. Forecast. Soc. Chang.* **2018**, *136*, 347–354. [[CrossRef](#)]
2. Tang, S.; Shelden, D.R.; Eastman, C.M.; Pishdad-Bozorgi, P.; Gao, X. A review of building information modeling (BIM) and the internet of things (IoT) devices integration: Present status and future trends. *Autom. Constr.* **2019**, *101*, 127–139. [[CrossRef](#)]
3. Verma, A.; Prakash, S.; Srivastava, V.; Kumar, A.; Mukhopadhyay, S.C. Sensing, Controlling, and IoT Infrastructure in Smart Building: A Review. *IEEE Sens. J.* **2019**, *19*, 9036–9046. [[CrossRef](#)]
4. Kim, T.-h.; Ramos, C.; Mohammed, S. Smart City and IoT. *Future Gener. Comput. Syst.* **2017**, *76*, 159–162. [[CrossRef](#)]
5. Theodoridis, E.; Mylonas, G.; Chatziagiannakis, I. Developing an IoT Smart City framework. In Proceedings of the IISA 2013, Piraeus, Greece, 10–12 July 2013; pp. 1–6.
6. Gaur, A.; Scotney, B.; Parr, G.; McClean, S. Smart City Architecture and its Applications Based on IoT. *Procedia Comput. Sci.* **2015**, *52*, 1089–1094. [[CrossRef](#)]
7. Latre, S.; Leroux, P.; Coenen, T.; Braem, B.; Ballon, P.; Demeester, P. City of things: An integrated and multi-technology testbed for IoT smart city experiments. In Proceedings of the 2016 IEEE International Smart Cities Conference (ISC2), Trento, Italy, 12–15 September 2016; pp. 1–8.
8. Memos, V.A.; Psannis, K.E.; Ishibashi, Y.; Kim, B.-G.; Gupta, B.B. An Efficient Algorithm for Media-based Surveillance System (EAMSuS) in IoT Smart City Framework. *Future Gener. Comput. Syst.* **2018**, *83*, 619–628. [[CrossRef](#)]
9. Razmjoo, A.; Gandomi, A.; Mahlooji, M.; Astiaso Garcia, D.; Mirjalili, S.; Rezvani, A.; Ahmadzadeh, S.; Memon, S. An Investigation of the Policies and Crucial Sectors of Smart Cities Based on IoT Application. *Appl. Sci.* **2022**, *12*, 2672. [[CrossRef](#)]
10. Anagnostopoulos, T.; Zaslavsky, A.; Medvedev, A. Robust waste collection exploiting cost efficiency of IoT potentiality in Smart Cities. In Proceedings of the 2015 International Conference on Recent Advances in Internet of Things (RIoT), Singapore, 7–9 April 2015; pp. 1–6.
11. Mohammadi, M.; Al-Fuqaha, A.; Guizani, M.; Oh, J.S. Semisupervised Deep Reinforcement Learning in Support of IoT and Smart City Services. *IEEE Internet Things J.* **2018**, *5*, 624–635. [[CrossRef](#)]
12. Mijač, M.; Picek, R.; Androcec, D. Smart City Services Driven by IoT: A Systematic Review. *J. Econ. Soc. Dev.* **2017**, *4*, 40–50.
13. Sadhukhan, P. An IoT based Framework for Smart City Services. In Proceedings of the 2018 International Conference on Communication, Computing and Internet of Things (IC3IoT), Chennai, India, 15–17 February 2018; pp. 376–379.
14. Bryant, N.; Spencer, N.; King, A.; Crooks, P.; Deakin, J.; Young, S. IoT and smart city services to support independence and wellbeing of older people. In Proceedings of the 2017 25th International Conference on Software, Telecommunications and Computer Networks (SoftCOM), Split, Croatia, 21–23 September 2017; pp. 1–6.
15. Jararweh, Y.; Otoum, S.; Ridhawi, I.A. Trustworthy and sustainable smart city services at the edge. *Sustain. Cities Soc.* **2020**, *62*, 102394. [[CrossRef](#)]
16. Jin, J.; Gubbi, J.; Marusic, S.; Palaniswami, M. An Information Framework for Creating a Smart City Through Internet of Things. *IEEE Internet Things J.* **2014**, *1*, 112–121. [[CrossRef](#)]
17. Jalali, R.; El-khatib, K.; McGregor, C. Smart city architecture for community level services through the internet of things. In Proceedings of the 2015 18th International Conference on Intelligence in Next Generation Networks, Paris, France, 17–19 February 2015; pp. 108–113.
18. Ahmad, M.W.; Mourshed, M.; Mundow, D.; Sisinni, M.; Rezugui, Y. Building energy metering and environmental monitoring—A state-of-the-art review and directions for future research. *Energy Build.* **2016**, *120*, 85–102. [[CrossRef](#)]
19. Bae, Y.; Bhattacharya, S.; Cui, B.; Lee, S.; Li, Y.; Zhang, L.; Im, P.; Adetola, V.; Vrabie, D.; Leach, M.; et al. Sensor impacts on building and HVAC controls: A critical review for building energy performance. *Adv. Appl. Energy* **2021**, *4*, 100068. [[CrossRef](#)]
20. Palomo-Vélez, G.; Perlaviciute, G.; Contzen, N.; Steg, L. Promoting energy sources as environmentally friendly: Does it increase public acceptability? *Environ. Res. Commun.* **2021**, *3*, 115004. [[CrossRef](#)]
21. Slade, R.; Bauen, A. Micro-algae cultivation for biofuels: Cost, energy balance, environmental impacts and future prospects. *Biomass Bioenergy* **2013**, *53*, 29–38. [[CrossRef](#)]

22. de Santoli, L.; Albo, A.; Astiaso Garcia, D.; Bruschi, D.; Cumo, F. A preliminary energy and environmental assessment of a micro wind turbine prototype in natural protected areas. *Sustain. Energy Technol. Assess.* **2014**, *8*, 42–56. [[CrossRef](#)]
23. Ye, C.; Liu, D.; Chen, P.; Cao, L.N.Y.; Li, X.; Jiang, T.; Wang, Z.L. An Integrated Solar Panel with a Triboelectric Nanogenerator Array for Synergistic Harvesting of Raindrop and Solar Energy. *Adv. Mater.* **2023**, *35*, 2209713. [[CrossRef](#)]
24. Mehrjerdi, H.; Hemmati, R.; Shafie-khah, M.; Catalão, J.P.S. Zero Energy Building by Multicarrier Energy Systems including Hydro, Wind, Solar, and Hydrogen. *IEEE Trans. Ind. Inform.* **2021**, *17*, 5474–5484. [[CrossRef](#)]
25. Glass, A.; Levermore, G. Micro wind turbine performance under real weather conditions in urban environment. *Build. Serv. Eng. Res. Technol.* **2011**, *32*, 245–262. [[CrossRef](#)]
26. Agüera-Pérez, A.; Palomares-Salas, J.C.; González de la Rosa, J.J.; Florencias-Oliveros, O. Weather forecasts for microgrid energy management: Review, discussion and recommendations. *Appl. Energy* **2018**, *228*, 265–278. [[CrossRef](#)]
27. Gould, C.; Edwards, R. Review on micro-energy harvesting technologies. In Proceedings of the 2016 51st International Universities Power Engineering Conference (UPEC), Coimbra, Portugal, 6–9 September 2016; pp. 1–5.
28. Sun, X.; Feng, Y.; Wang, B.; Liu, Y.; Wu, Z.; Yang, D.; Zheng, Y.; Peng, J.; Feng, M.; Wang, D. A new method for the electrostatic manipulation of droplet movement by triboelectric nanogenerator. *Nano Energy* **2021**, *86*, 106115. [[CrossRef](#)]
29. Zhang, M.; Bao, C.; Hu, C.; Huang, Y.; Yang, Y.; Su, Y. A droplet-based triboelectric-piezoelectric hybridized nanogenerator for scavenging mechanical energy. *Nano Energy* **2022**, *104*, 107992. [[CrossRef](#)]
30. Vasiliev, M.; Nur-E-Alam, M.; Alameh, K. Recent Developments in Solar Energy-Harvesting Technologies for Building Integration and Distributed Energy Generation. *Energies* **2019**, *12*, 1080. [[CrossRef](#)]
31. Hemida, H.; Šarkić, A.; Vita, G.; Kostadinovic Vranesevic, K.; Höffer, R. On the Flow over High-rise Building for Wind Energy Harvesting: An Experimental Investigation of Wind Speed and Surface Pressure. *Appl. Sci.* **2020**, *10*, 5283. [[CrossRef](#)]
32. Ilyas, M.A.; Swingler, J. Piezoelectric energy harvesting from raindrop impacts. *Energy* **2015**, *90*, 796–806. [[CrossRef](#)]
33. Wong, C.-H.; Dahari, Z.; Abd Manaf, A.; Miskam, M.A. Harvesting Raindrop Energy with Piezoelectrics: A Review. *J. Electron. Mater.* **2015**, *44*, 13–21. [[CrossRef](#)]
34. Morabito, A.; Hendrick, P. Pump as turbine applied to micro energy storage and smart water grids: A case study. *Appl. Energy* **2019**, *241*, 567–579. [[CrossRef](#)]
35. Lee, J.H.; Kim, S.Y.; Kim, T.Y.; Khan, U.; Kim, S.-W. Water droplet-driven triboelectric nanogenerator with superhydrophobic surfaces. *Nano Energy* **2019**, *58*, 579–584. [[CrossRef](#)]
36. Munirathinam, P.; Anna Mathew, A.; Shanmugasundaram, V.; Vivekananthan, V.; Purusothaman, Y.; Kim, S.-J.; Chandrasekhar, A. A comprehensive review on triboelectric nanogenerators based on Real-Time applications in energy harvesting and Self-Powered sensing. *Mater. Sci. Eng. B* **2023**, *297*, 116762. [[CrossRef](#)]
37. Zhang, N.; Gu, H.; Lu, K.; Ye, S.; Xu, W.; Zheng, H.; Song, Y.; Liu, C.; Jiao, J.; Wang, Z.; et al. A universal single electrode droplet-based electricity generator (SE-DEG) for water kinetic energy harvesting. *Nano Energy* **2021**, *82*, 105735. [[CrossRef](#)]
38. Ding, J.; Tao, W.-Q.; Fan, S.-K. Study of vibrational droplet triboelectric nanogenerator on structural and operational parameters. *Nano Energy* **2020**, *70*, 104473. [[CrossRef](#)]
39. Xie, X.; Gou, Z. Obstacles of Implementing Green Building in Architectural Practices. In *Green Building in Developing Countries: Policy, Strategy and Technology*; Gou, Z., Ed.; Springer International Publishing: Cham, Switzerland, 2020; pp. 33–47.
40. Esa, M.R.; Marhani, M.A.; Yaman, R.; Hassan, A.A.; Hanisah, H.; Rashid, N.; Adnan, H. Obstacles in Implementing Green Building Projects in Malaysia. *Aust. J. Basic Appl. Sci.* **2011**, *5*, 1806–1812.
41. Wu, H.; Mendel, N.; van den Ende, D.; Zhou, G.; Mugele, F. Energy Harvesting from Drops Impacting onto Charged Surfaces. *Phys. Rev. Lett.* **2020**, *125*, 078301. [[CrossRef](#)] [[PubMed](#)]
42. Zou, H.; Zhang, Y.; Guo, L.; Wang, P.; He, X.; Dai, G.; Zheng, H.; Chen, C.; Wang, A.C.; Xu, C.; et al. Quantifying the triboelectric series. *Nat. Commun.* **2019**, *10*, 1427. [[CrossRef](#)] [[PubMed](#)]
43. Zhan, F.; Wang, A.C.; Xu, L.; Lin, S.; Shao, J.; Chen, X.; Wang, Z.L. Electron Transfer as a Liquid Droplet Contacting a Polymer Surface. *ACS Nano* **2020**, *14*, 17565–17573. [[CrossRef](#)] [[PubMed](#)]
44. Xi, Y.; Wang, J.; Zi, Y.; Li, X.; Han, C.; Cao, X.; Hu, C.; Wang, Z. High efficient harvesting of underwater ultrasonic wave energy by triboelectric nanogenerator. *Nano Energy* **2017**, *38*, 101–108. [[CrossRef](#)]
45. Zhang, Q.; Jiang, C.; Li, X.; Dai, S.; Ying, Y.; Ping, J. Highly Efficient Raindrop Energy-Based Triboelectric Nanogenerator for Self-Powered Intelligent Greenhouse. *ACS Nano* **2021**, *15*, 12314–12323. [[CrossRef](#)] [[PubMed](#)]
46. Zeng, Y.; Luo, Y.; Lu, Y.; Cao, X. Self-powered rain droplet sensor based on a liquid-solid triboelectric nanogenerator. *Nano Energy* **2022**, *98*, 107316. [[CrossRef](#)]
47. Zheng, Y.; Liu, T.; Wu, J.; Xu, T.; Wang, X.; Han, X.; Cui, H.; Xu, X.; Pan, C.; Li, X. Energy Conversion Analysis of Multilayered Triboelectric Nanogenerators for Synergistic Rain and Solar Energy Harvesting. *Adv. Mater.* **2022**, *34*, 2202238. [[CrossRef](#)]
48. Li, Z.; Cao, B.; Zhang, Z.; Wang, L.; Wang, Z.L. Rational TENG arrays as a panel for harvesting large-scale raindrop energy. *iEnergy* **2023**, *2*, 93–99. [[CrossRef](#)]
49. Deng, W.; Libanori, A.; Xiao, X.; Fang, J.; Zhao, X.; Zhou, Y.; Chen, G.; Li, S.; Chen, J. Computational investigation of ultrasound induced electricity generation via a triboelectric nanogenerator. *Nano Energy* **2022**, *91*, 106656. [[CrossRef](#)]
50. Qian, H.; Mao, Y.; Xiang, W.; Wang, Z. Recognition of human activities using SVM multi-class classifier. *Pattern Recognit. Lett.* **2010**, *31*, 100–111. [[CrossRef](#)]

51. Biau, G.; Scornet, E. A random forest guided tour. *TEST* **2016**, *25*, 197–227. [[CrossRef](#)]
52. Gilliland, F.D. Outdoor air pollution, genetic susceptibility, and asthma management: Opportunities for intervention to reduce the burden of asthma. *Pediatrics* **2009**, *123*, S168–S173. [[CrossRef](#)]

**Disclaimer/Publisher’s Note:** The statements, opinions and data contained in all publications are solely those of the individual author(s) and contributor(s) and not of MDPI and/or the editor(s). MDPI and/or the editor(s) disclaim responsibility for any injury to people or property resulting from any ideas, methods, instructions or products referred to in the content.